Intracellular actin-based transport: How far you go depends on how often you switch

Joseph Snider*, Francis Lin*, Neda Zahedi†‡, Vladimir Rodionov†, Clare C. Yu*§, and Steven P. Gross*§¶‖

Departments of *Physics and Astronomy and ¶Developmental and Cell Biology, University of California, Irvine, CA 92697; †Center for Biomedical Imaging Technology, 263 Farmington Avenue, MC1507, Farmington, CT 06032-1507; and ‡Randall Centre for Molecular Mechanisms of Cell Function, King's College London, Guy's Campus, London Bridge, London SE1 1UL, United Kingdom

Edited by Charles F. Stevens, The Salk Institute for Biological Studies, La Jolla, CA, and approved July 19, 2004 (received for review May 3, 2004)

Intracellular molecular motor-driven transport is essential for such diverse processes as mitosis, neuronal function, and mitochondrial transport. Whereas there have been *in vitro* studies of how motors function at the single-molecule level, and *in vivo* studies of the structure of filamentary networks, studies of how the motors effectively use the networks for transportation have been lacking. We investigate how the combined system of myosin-V motors plus actin filaments is used to transport pigment granules in *Xenopus* melanophores. Experimentally, we characterize both the actin filament network, and how this transport is altered in response to external signals. We then develop a theoretical formalism to explain these changes. We show that cells regulate transport by controlling how often granules switch from one filament to another, rather than by altering individual motor activity at the single-molecule level, or by relying on structural changes in the network.

Intracellular transport of various cargos is essential for proper cell function, yet the principles regulating cargo motion are still not well understood. Whereas thermal diffusion is sufficient for the transportation of many small molecules, e.g., ATP or acetyl CoA, larger cargos require an active transit system. Such intracellular transport is present in all eukaryotic cells and is realized by a system of polymerized filaments [actin filaments (AFs) and microtubules (MTs)] and molecular motors [myosin-V (M-V), kinesin, dynein, etc.], not unlike roadways and trucks. The general model (1) is that the orderly MT filaments provide long-distance transport from the periphery to the nucleus or *vice versa*, in a fairly linear manner. In conjunction, AFs provide local transport from the MT superhighways to the remainder of the cell (2). Whereas there have been careful studies of single-motor properties as well as of the structure of the filamentary networks, there are deficiencies in our understanding of how those components work together to provide efficient, reliable transport. In this paper, we show that cells can change the way they transport cargo predominantly by changing the way the cargos use the network, rather than by changing individual motor properties, or by relying on changes to the structure of the filamentary networks.

To make general transport into a tractable problem, we simplify it considerably and study it within the context of the *Xenopus* melanophore model system. The skin cells of this system are adapted for color camouflage by either moving pigment granules to the vicinity of the center of the cell in a process called aggregation, or by distributing them uniformly throughout the cell in a process known as dispersion (1). Because these cells are very nearly two-dimensional and the half-micrometer pigment granule cargos are easily discerned, they are an ideal system in which to observe active transport with single-particle tracking. Because MTs are long, radially arranged filaments, there is less uncertainty about how MT-based transport works compared with transport on AFs. Thus, we eliminate MTs and focus on understanding transport on actin by means of the molecular motor, M-V. By using single-particle tracking, we find that the mean square displacement of cargos after a given amount of time is much larger during dispersion than during aggregation. We show that this change is not due to altering the speed of the M-V motors, nor can changes in the structure of the actin network account for this change. By combining a theoretical diffusion model and a numerical simulation, we show that this change in intracellular transport is controlled by altering the probability for a cargo to switch from filament to filament.

Tracking Data

Individual cargos were tracked in cells that lacked MTs and only had AFs. Thus, cargo motion appeared to be quasi-Brownian over long periods of time, although cargos could instantaneously move linearly along an AF. Cells were either treated with melatonin to induce aggregation or with melanocyte-stimulating hormone to induce dispersion (1). We analyze transport by measuring the average of the square of the displacement as a function of time $\langle r^2(t)\rangle$ (Fig. 1), as in previous work (1). Our work extends previous data (1) two to four times longer, allowing the observation at long times of Brownian motion, where $\langle r^2\rangle$ is linear in time. Two features of Fig. 1 are especially striking: the crossover from positive curvature at short times to long-time linear behavior and the difference in the magnitude of $\langle r^2\rangle$ for dispersion and aggregation. The positive curvature of $\langle r^2\rangle$ at short times indicates that ordinary diffusion does not hold. There are two more general forms of anomalous diffusion that we can consider (3). The first is power-law diffusion with $\langle r^2(t)\rangle = At^\lambda$ for constant A and power $\lambda>1$ (4). Alternatively, suppose the motors haul the cargos along a filament for some distance and then turn onto a new filament. In this case, a Langevin form associated with the solution of the Langevin equation is a reasonable interpolation formula between linear motion at short times and diffusion at long times (5):

$$\langle r^2(t)\rangle = D\left[t - \tau\left(1 - \exp - \frac{t}{\tau}\right)\right] \qquad [1]$$

where D is a diffusion coefficient and τ sets a time scale for crossover from short- to long-time behavior. Note that some authors place an arbitrary factor of 4 in front of the D. Treating Eq. **1** as a fitting function, a time scale τ is introduced, which separates short-time ($t<\tau$) linear motion ($\langle r^2\rangle \sim t^2$) and long-time ($t > \tau$) diffusive motion ($\langle r^2\rangle \sim t$). It should be noted that the existence of the AF network makes other fitting forms possible (6, 7), but the two mentioned here are reasonably general.

To distinguish which functional form is best for modeling, we fit both equations to the data on time ranges of [0,2], [0,4], . . . , s. The parameters are plotted versus the size of the time range, in Fig. 2. After a fairly rapid rise, the Langevin fits (Fig. 2 *A* and

This paper was submitted directly (Track II) to the PNAS office.

Abbreviations: AF, actin filament; MT, microtubule; M-V, myosin-V; EM, electron micrograph; MFP, mean free path.

§C.C.Y. and S.P.G. contributed equally to this work.

‖To whom correspondence should be addressed. E-mail: sgross@uci.edu.

www.pnas.org/cgi/doi/10.1073/pnas.0403092101

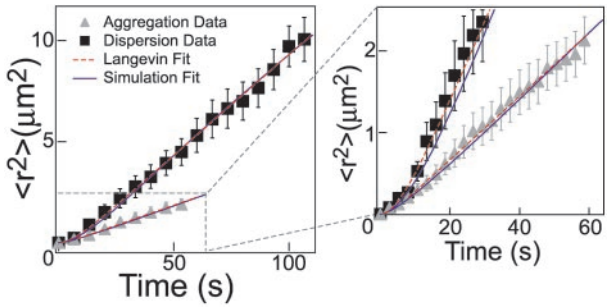

Fig. 1. Particle tracking data and fits for aggregation (70 tracks) and dispersion (40 tracks). For clarity, only every 50th data point is shown in *Left* and every 20th in *Right*. The error bars represent errors from the tracking. As described in the text, the solid (blue) lines are fits to simulations, and the dashed (red) lines are fits to the Langevin solution. (*Right*) A magnification of the aggregation region is shown on to emphasize the fits, errors, and short-time curvature.

B) converge to fixed values, but the power-law fits (Fig. 2 *C* and *D*) do not converge on the available time scale. Thus, because it depends less strongly on the amount of data taken, the Langevin form is preferred. The fit parameters at the longest time are presented in Table 1.

One remaining problem is that at short times the power λ should be 2 to be fully consistent with the Langevin equation, instead of the smaller value seen in Fig. 2*D*. This discrepancy is possibly due to colliding or immobile cargos at short times.

Furthermore, at long times, one might expect the power to be 1 rather than ≈1.2, but this is just an artifact of the system being at $\approx 20\tau$ at the longest times because a fit of a power law to a Langevin function from 0 to 20 τ gives an apparent exponent of ≈1.1. Finally, the Langevin equation technically models a system in thermal equilibrium, which is not true for the M-V motors because they are actively hydrolyzing ATP. However, assuming the M-V motors are moving smoothly in steady state, the resulting constant kinetic energy of the cargos can be treated as an effective temperature consistent with the Langevin formalism. Thus, despite the possible deficiencies at short times, Eq. **1** seems consistent with both the aggregation and dispersion data, and, as will be seen below, it is especially convenient for inferring the motion of individual cargos from their average. However, we will be careful to never rely solely on Eq. **1** and the Langevin formalism from which it came, but we will rely on them to some extent to verify results from other approaches.

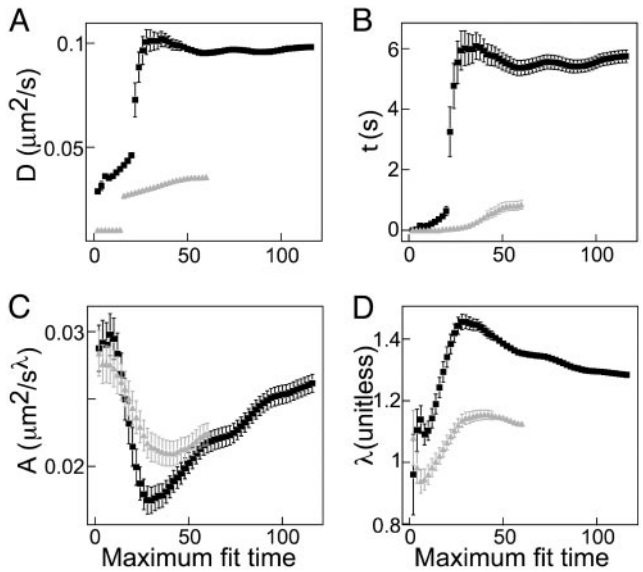

Fig. 2. Fit parameters versus maximum fit time. (*A*) The Langevin parameter *D*. (*B*) The parameter τ. (*C*) T coefficient *A* from the power-law fit. (*D*) The power-law exponent λ. Gray triangles, aggregation; black squares, dispersion. Note that the Langevin parameters have converged, whereas the power-law parameters are not conclusive.

Table 1. Fit parameters for Langevin interpretation

State of cell	D, $\mu m^2/s$	τ, s
Dispersion	0.0984 ± 0.0007	5.9 ± 0.2
Aggregation	0.0388 ± 0.0006	2.9 ± 0.3

Errors are from the fit.

Interestingly, we find that the cargos' speed does not change much between dispersion and aggregation. The speed is calculated from the cargo's average displacement over a short time. Some care is required because the tracking error is comparable to the separation between tracking points, causing a systematic error (see Figs. 8 and 9 and *Supporting Text*, which are published as supporting information on the PNAS web site). The corrected speeds are $v_a = 72 \pm 4$ nm/s for aggregation and $v_d = 80 \pm 5$ nm/s for dispersion, which agree within errors. Because of the complexity of the tracking error, the speeds are also calculated from the fits to Eq. **1**. From the Langevin formalism, we can approximate the speed of the particle as given by $\langle v \rangle \approx \sqrt{D/2\tau}$. Plugging in numbers from Table 1 gives $v_a = 82 \pm 4$ nm/s and $v_d = 91 \pm 2$ nm/s, which is in reasonable agreement with the more direct measurements. Some of the overestimate in the Langevin speeds can be explained by the reliance on the approximation $\langle v^2 \rangle \approx \langle v \rangle^2$. The fact that the Langevin estimates are comparable to the speeds determined from particle tracking means that both approaches are giving reasonable estimates for the speed. Thus, the cargo speeds do not change significantly from aggregation to dispersion. This result implies that the large difference between aggregation and dispersion must be generated not by changes in the speed of individual cargos, but by cargo interactions with the filament system.

A useful parameter that characterizes the motion of cargos is the mean free path (MFP) which is the average distance a cargo travels in a straight line, or on a single filament. First, the MFP is estimated directly from the tracks used to find $\langle r^2 \rangle$. Each track is a set of points that correspond to the position of a single cargo over time. As already mentioned, the tracks consist of linear sections, where the cargos are traveling along a single filament, and sharp turns, where cargos switch to a new filament. The position of the sharp turn from one filament to another (turning point) for a given track is found by examining the tracks by hand and estimating the positions. This procedure is performed for a sample of the tracks: aggregation, 17 tracks with 154 total turning points; dispersion, 30 tracks with 195 total turning points. Then, the average distance between turning points is calculated and is the MFP. In aggregation, it is 260 ± 20 nm, and in dispersion, it is 600 ± 40 nm, where the error is the SE of the mean. Because the location of the turning points is found by hand, the error estimates may be unreliable.

The Langevin formalism provides an alternate measurement of the MFP by multiplying the speeds by the time τ to give 237 ± 12 nm (aggregation) and 539 ± 9 nm (dispersion). These findings agree well with the direct measurements and have both more reliable error estimates and use of all of the tracks. It is somewhat surprising that the Langevin formalism works so well in this case, because, as noted before, the physical basis for using Langevin is somewhat shaky. However, its excellent agreement with direct measurements of both the speeds from before and the MFP here show that the Langevin formalism captures the essential physics

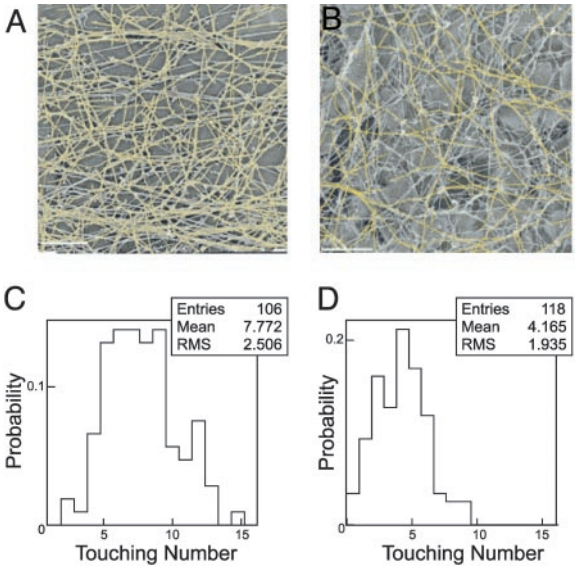

Fig. 3. Quantification of actin filament network. (*A*) EM of an aggregating cell; actin is yellow. (*B*) EM of a dispersing cell. The scale bars (white) are 1 μm long. Platinum replica EM was performed as described (21). (*C*) Distribution of the number of filaments reachable by a randomly placed cargo during aggregation. (*D*) The same as in *C*, during dispersion.

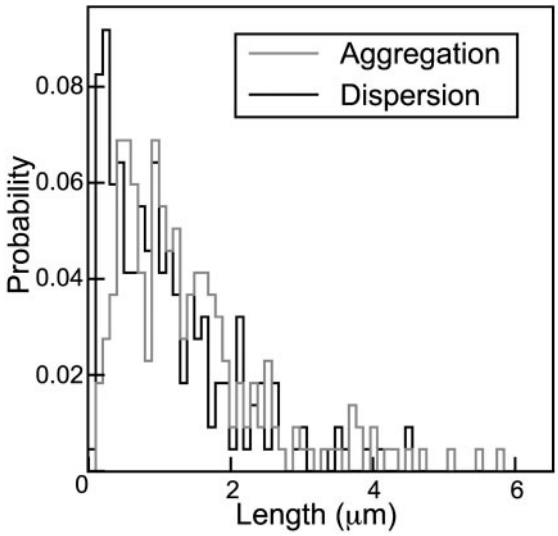

Fig. 4. Measured probability of finding an AF of a given length. Data are the same for aggregation and dispersion. The mean length is ≈1.3 μm.

of the situation. Also, the Langevin formalism very quickly and easily gives results that are otherwise torturously difficult to estimate.

Electron Micrographs (EMs)

The MFP can also be deduced from the AF network seen in EMs taken of fixed cells (Fig. 3 *A* and *B*). Because single M-V motors are processive over long ranges ($D_{\text{avg}} > 1{,}600$ nm; ref. 8), the cargo is likely to change direction not because the motor randomly falls off the filament, but instead because either the filament ends or the cargo switches to moving along a different filament. Thus, the structure of the AF network could determine the MFP of a cargo in two ways. In the first scenario, a cargo starts randomly on a filament, goes to the end, falls off, and attaches to a new filament. In this case, the average distance traveled on a filament (equivalently, the MFP) is the average filament length $\bar{L}$ divided by 2, because the cargo starts at every point on the filament with equal probability. Here, $\bar{L} = 1{,}300 \pm 200$ nm (Fig. 4), giving an approximate MFP of 650 ± 100 nm, where the errors are estimated from Fig. 4.

In the second scenario, the cargo may switch from one filament to another where the two filaments cross. Define p_s as the probability to switch at a filament and d_I the average distance between filament intersections. Assuming the filaments are infinitely long and that the cargos start at intersections, the MFP is the initial d_I to the first intersection ahead, plus an additional d_I for each skipped intersection. The average number of skipped turnings is $1/p_s$ (see *Supporting Text*). Thus, the MFP is d_I/p_s. For p_s less than some value, the MFP will be larger than half a filament, and the assumption of an infinite filament breaks down. In this case, the first scenario applies and the MFP is $\bar{L}/2$. For simplicity our MFP estimate of d_I/p_s ignores what happens at the ends of the filaments. Including end effects makes the problem analytically intractable, and we will turn to simulations below to handle them. We can measure d_I directly by drawing straight lines of a given length and counting the number of times they intersected and AF. This result shows a distance of $d_I = 160 \pm 40$ nm during aggregation and $d_I = 330 \pm 70$ nm during dispersion, reflecting an apparent change in density seen in Fig. 3 *A* and *B*.

Unfortunately, the value of p_s is not independently known in aggregation or dispersion, but for an initial estimate, we can require the rough formula for the MFP from the EMs to match the MFPs already calculated. In aggregation, the MFP derived from the Langevin fit is less than half of a filament length, implying a non-zero switching probability between filaments. We calculate this probability by $p_s = d_I/MFP \sim 70\%$, where $\sim$ indicates that this rough estimate ignores end effects. In dispersion, the Langevin-calculated MFP is approximately $\bar{L}/2$, implying that the cargos only switch when they reach the end of their current AF. Thus, p_s is effectively zero, although it could be as high as 30% and still traverse an entire filament without turning. This change in the calculated value of p_s indicates that the cargos change directions more often during aggregation than during dispersion.

Another feature of the EMs in Fig. 3 is the change in the density of the AF network between the aggregation and dispersion cases. Experimentally, this result was quantified by randomly placing circles on the EM images and counting the intersecting AFs, defined as the touching number n_t. The circles have a diameter of 568 nm because the average cargo diameter is 568 ± 72 nm. $n_t = 7.8 \pm 2.5$ (mean $\pm$ rms) during aggregation (Fig. 3*C*), and $n_t = 4.2 \pm 1.9$ during dispersion (Fig. 3*D*). Because the statistics are low (three cells for aggregation and two for dispersion), we avoid general conclusions about density, and investigate the significance of changes in filament density by using computer simulations (see below).

Interestingly, during dispersion where the density appears lower, the minimum expected touching number is ≈2, corresponding to the current filament and the one onto which a cargo switches. Thus, the cell could be minimizing the total number of filaments, it creates subject to the constraint that at least one new filament is available (to avoid stranded cargos). We should mention that quantitative measurements of fluorescence in phalloidin-stained cells failed to detect a difference in the total amount of polymerized actin between aggregated and dispersed cells, although in principle, changes in bundling could alter the effective AF density without changing total polymer mass. Definitively determining whether the actin cytoskeleton is altered between aggregation and dispersion is certainly interest-

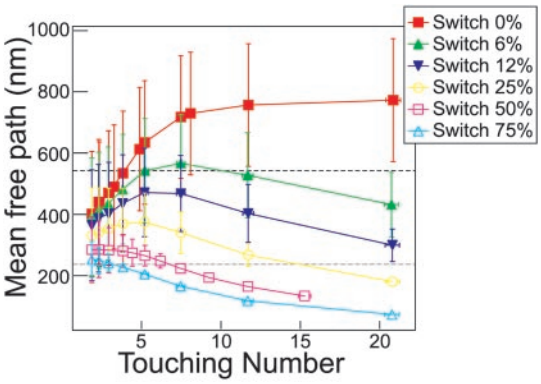

Fig. 5. MFP calculated from simulations at various switching probabilities and touching numbers. Errors reflect both the SD of the separate runs and the error in the measured filament length, as weighted by the probability to get to the end. The dashed lines represent the MFP values from the Langevin formalism; dark (*top*) is dispersion, and light (*bottom*) is aggregation. Note that varying density (touching number) alone is insufficient to vary the MFP over the experimentally observed range.

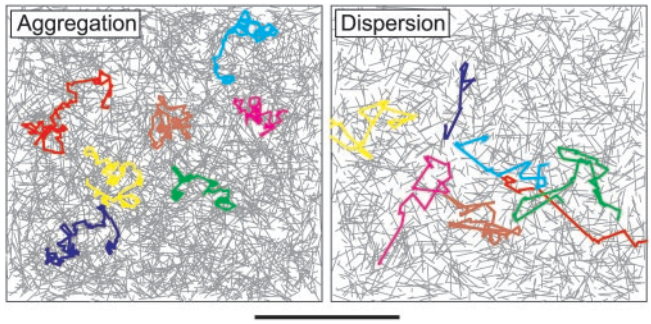

Fig. 6. Sample simulation data for aggregation (*Left*) and dispersion (*Right*). The colored lines represent paths taken by sample walkers and the gray lines represent filaments. (Bar, 10 μm.) All walkers took 1,000 steps or walked for ≈500 s. Note that aggregation paths (*Left*) tend to be local and clumped, whereas dispersion paths (*Right*) tend to be spread out and spindly. For aggregation, we set p_s = 50% and n_t = 7.8; and for dispersion, we set p_s = 0% and n_t = 4.2.

ing, but a careful study of this question is beyond the scope of this predominantly theoretical paper.

Simulations

The simplistic model of infinite filament lengths in the previous section suggests that a more realistic numerical model is worthwhile. We combine the EMs and the known properties of M-V to build such a model. In our simulations, AFs are represented by unidirectional straight lines with lengths chosen from Fig. 4. Simulated AFs are placed randomly on a circular region of radius $R \gg \bar{L}$, representing an idealized cell's extended cytoplasm. The density is adjusted by fixing the number of simulated AFs and varying R. Cargos are placed on the network and are allowed to switch either to an intersecting AF or, if they reach the end, to any AF within reach. More simulation details are in Fig. 10, which is published as supporting information on the PNAS web site, and *Supporting Text*, but the best analogy to follow is one of walkers attached to and moving on a network of one-way roads.

One simplification is that moving cargos only switch onto new AFs that physically cross their current AF, ignoring any other AFs within reach. This conclusion is reasonable because processivity along an AF requires at least one properly attached and functioning M-V. Thus, for a different motor to pull the cargo onto a new AF, it has to both find a new AF and unbind the current motor. At physical AF crossings, the M-V activity is possibly interrupted and a new AF is guaranteed to be nearby, heightening the chance to switch. Thus, crossings are well modeled by a switching probability p_s. Finally, at filament ends, any filament within reach is accessible because thermal energy is sufficient to rotate the cargo rapidly, giving its motors ample opportunity to attach to a new filament (9).

The simulations model the combined effects of switching probability and filament density on the cargos' transport by independently varying them about the EM values. For each p_s and density, we run 100 network realizations, each with 1,000 trials. The MFP is calculated by directly tracking the distance between turns and averaging (Fig. 5). As a means of verification, the $\langle r^2 \rangle$ (see below) is also fit to a Langevin form, and the subsequent MFP agrees with the direct measurement from the simulations. Note that this verification provides support for using Langevin as an interpolation form in the first place.

Two important conclusions are drawn from this simulation. First, (see Fig. 5) when the simulations were done at the experimentally determined touching numbers n_t (aggregation, 7.8 ± 2.5; dispersion, 4.2 ± 1.9), to achieve MFPs that matched the Langevin-fit derived values (aggregation, 237 ± 12 nm; dispersion, 539 ± 9 nm), it was necessary to use switching p_s of 50 ± 15% for aggregation and 6 ± 6% for dispersion, where errors are estimated from Fig. 5. These values are consistent with the rough estimates taken directly from the EMs (aggregation, ≈70%; dispersion, less than ≈30%) as well as the direct experimental measurements of the MFPs, but the simulated values include AF end effects and so are more reliable. Thus, the simulations confirm the original Langevin study that suggested that the probability of switching between filaments is different in aggregation and dispersion.

Second, surprisingly, varying the density alone does not explain the experimentally observed variation in MFP. For instance, from Fig. 5 we can see that under the assumption of 50% switching, it is not possible to achieve a dispersion-like MFP by altering filament density. Similarly, to be able to attain an aggregation-like MFP requires at least a 25% chance to switch filaments, even at filament densities much higher than experimentally observed (i.e., n_t = 15). Finally, by altering switching probability alone but keeping filament density constant (e.g., n_t = 5) it is possible to achieve both dispersion-like and aggregation-like MFPs. Therefore, control of AF-based transport is achieved by tuning the switching probability p_s, with alteration of density being less important or possibly even irrelevant.

To build intuition about the effects of various p_s, a sample plot of simulated paths ("trajectories") of individual granules in aggregation and dispersion is seen in Fig. 6. In general, during aggregation (Fig. 6 *Left*), the cargo frequently switches from filament to filament, giving short, randomly oriented steps leading to clumped trajectories that sample the local neighborhood. Instead, during dispersion (Fig. 6 *Right*), switching only occurs at the end of the filaments, making the paths appear long and spindly, and is effective at spreading out the cargos.

To be more quantitative, $\langle r^2 \rangle$ is measured in simulations with 100 network realizations, each with 1,000 trials, for aggregation (p_s = 50% and n_t = 7.8) and dispersion (p_s = 0% and n_t = 4.2). The simulation length scale is already in nanometers, but the time scale is in arbitrary time steps TS. To convert from TS to seconds, the simulated $\langle r^2 \rangle$'s time is scaled onto the experimental $\langle r^2 \rangle$'s time (Fig. 1). This scaling gives 2.1 ± 0.1 TS/s for aggregation and 2.0 ± 0.1 TS/s for dispersion. The scaling is checked with the speed. Converting from the fixed simulation value of 37 nm/TS (10) to units of nm/s gives v_a = 78 ± 2 nm/s and v_d = 74 ± 2 nm/s. Aggregation agrees with previous estimates, but dispersion is ≈10% lower than expected, probably reflecting a slightly non-zero p_s. As another means of verifica-

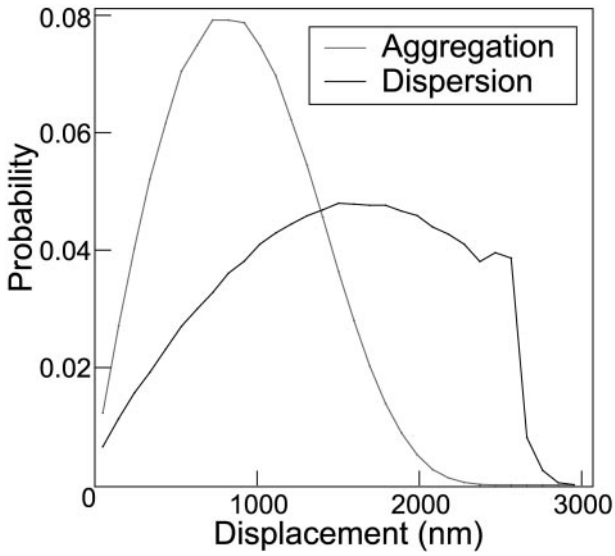

Fig. 7. Displacement histograms from simulations of aggregation and dispersion after 30 s (real time) of diffusion. The small bump in the line near R = 2,500 nm in the dispersion line is from cargos that traveled along only one filament and accounts for <1% of the total probability.

tion, the simulated $\langle r^2 \rangle$ is also fit to a Langevin form, and the speed is calculated. In this case, the speeds are $v_a = 37.8 \pm 0.1$ nm/TS and $v_d = 38.38 \pm 0.03$ nm/TS. Both cases overestimate the actual speed (37 nm/TS) by up to 4% due to the approximation of $\langle v^2 \rangle \approx \langle v \rangle^2$. This result lends credence to the earlier claim that the Langevin speeds are systematically too large.

Finally, the cargos' displacement after 30 s (real time) is tracked to verify that the net magnitude of the motion is reasonable. The distribution (Fig. 7) shows that aggregating cargos tend to stay within 700 nm of their origin, whereas dispersing cargos spread out more evenly over a range of 500–2,700 nm, verifying the intuitive picture of Fig. 6. Experimentally, inter-MT spacing is ≈800 nm, estimated from a figure in ref. 1. Thus, in a reasonably short time, the M-V-driven motion finds an MT during aggregation, and spreads out the cargos evenly over the region between MTs during dispersion. Note that by having a large characteristic time τ, the dispersing cargos stay in the short-time diffusion regime longer. Thus, compared with aggregating cargos, the dispersing cargos spread themselves out with a distribution that remains fairly flat for much longer times (and distances). Therefore, we have verified that dispersing cargos do indeed perform better at the task of spreading out than do aggregating cargos.

Discussion

Thus far, experiments combined with simulations provide a consistent picture of the intracellular transport on AF networks. Specifically, cargo transport on the AF network is not controlled by varying the speeds of the cargos, but instead is controlled by the probability that a cargo switches filaments at an intersection. This finding leads to the conclusion that the MFP of cargos in dispersion is much longer than that of aggregation. By using these MFPs, the simulations indicate a switching probability close to 0% during dispersion, and $p_s \approx 50\%$ during aggregation. An accompanying change in filament density can in principle fine-tune the motion. Also, we verified that by remaining in the short time diffusion regime for a relatively long time, dispersing cargos spread themselves out more uniformly than aggregating cargos.

Two further questions will be addressed here. First, it is not clear that aggregating cargos are in any way superior to dispersing cargos in terms of finding an MT, although some simple simulations seem to indicate that they have a slight edge over dispersion (see *Supporting Text*, and Fig. 11, which is published as supporting information on the PNAS web site). In any case, it is clear that the motion during aggregation is at least neutral as far as finding an MT goes when compared with dispersion. Thus, the change in motion may be important, but could also be a side effect of a different feature.

Second, we hypothesize that p_s is controlled by changing the number of active motors, from one active M-V motor during aggregration to two active motors during dispersion. From *in vivo* force measurements on two other systems, 6–10 pN of force stalls typical MT-driven transport (11, 12). Further, *in vitro* experiments on kinesin show that an opposing force of approximately half the stall force reduces the kinesin-driven travel velocity by 50% (13), and other work suggests that dynein's response to load is likely similar (14). During dispersion, M-V function decreases plus-end and minus-end MT-based transport velocities by ≈40% (1). Thus, the cargo's M-V motors oppose MT motion with a force of ≈3–5 pN. Individual M-Vs *in vitro* can exert a maximum of 2–3 pN (8, 15). Hence, two M-V motors must be active to account for the calculated ≈3–5 pN force. In contrast, during aggregation, MT-based transport dominates actin-based motion without slowing down (1). Thus, it is likely that only one M-V motor is active at a time. Unfortunately, a direct measurement of stalling force in the Melanophore system is difficult because the pigment granules are colored and strongly absorb optical trap laser light, heat up, and literally explode.

The 1 ↔ 2 motor hypothesis is also consistent with the previously measured change in the total number of M-V motors on a cargo from ≈60 (aggregation) to ≈90 (dispersion; ref. 1). A number of testable factors could contribute to this relatively low utilization. First, *in vivo* estimates of AF to M-V binding rates are not well known so many M-Vs may be required for any to be processive. Second, in some cases there are proteins present on the cargo that inactivate M-V, possibly limiting the activity (16). Third, M-V may be localized on one part of the cargo, resulting in many M-Vs that are out of reach of an AF (17, 18). Finally, the 1 ↔ 2 motor hypothesis is consistent with p_s, switching from ≈50% to ≈0%. Away from AF–AF intersections, any attempts to switch filaments is inhibited by the motion of the active M-V, as already mentioned. At intersections, when only one M-V is active it can be easily interrupted, giving any other M-Vs a chance to pull the cargo onto a new filament. Assuming an average of two filaments per intersection gives $p_s \approx 50\%$, corresponding to aggregation. Instead, if two motors are active then at least one is always driving the cargo forward, so the cargo has little chance to switch. In other words, another M-V trying to pull the cargo onto a new filament would be unlikely to overpower the two M-Vs already attached to the current filament. This result gives $p_s \approx 0\%$, corresponding to dispersion. Therefore, the 1 ↔ 2 motor hypothesis provides a mechanism for the cell to control the switching probability and hence the diffusive motion.

How generally applicable are these findings? We have modeled the AFs as a directed but randomly oriented network. This conclusion appears to be true in the case of the melanophore system, yet in many systems, the prevailing notion is that the AFs are not random but instead are all pointing toward the plasma membrane. However, this notion is likely incomplete. Typically, the directionality and organization of the actin cytoskeleton has been quantified in motile cells such as fibroblasts, especially close to the leading edge (i.e. the edge causing motility), because the goal has been to understand cell motility. Nonetheless, most cells are not actively crawling. In such cells, less is known about the actin organization, especially away from the plasma membrane (here we ignore yeast, because for long-distance transport they exclusively use actin cables, unlike mammalian cells that use MTs). In such nonmotile mammalian cells, it seems likely that

many of the AFs are relatively randomly organized, similar to the melanophore cells. We were not able to find much published data, but one important case where our supposition appears correct is in nerve growth cones (19). Thus, it seems likely that the model, we have developed here has relevance to many AF-based vesicular transport systems, whenever the transport is occurring away from the plasma membrane. For instance, similar $\langle r^2 \rangle$ versus time motion of influenza viruses in endosomes moving along AFs has recently been reported (20).

Conclusions

In conclusion, we have examined the motion of cargos moving on AF networks through M-V motors. We find that the mean square displacement of cargos after a given amount of time is much larger during dispersion than during aggregation. This change is not due to altering the speed of the M-V motors, nor can changes in the structure of the actin network account for it. This experimentally measured change can be explained through simulations and a Langevin interpolation model, combined with measurements from EMs of the AF network. Together, these measurements show that the cell controls motion by altering the likelihood of switching from one AF to another with a switching probability of ≈50% during aggregation and ≈0% during dispersion. We hypothesize that this is the result of changing the number of active M-V motors from one during aggregation to two during dispersion. We speculate that during dispersion the transport is optimized for fast, even spreading.

We thank A. Lander for comments on the manuscript. This work was supported by National Institute of General Medical Sciences Grant GM-64624-01 (to S.P.G.), National Institute of General Medical Sciences Grant GM-62290-01 (to V.R), National Center for Research Resources Grant RR13186 (to V.R.), and U.S. Department of Energy Grant DE-FG03-00ER45843 (to C.C.Y.).

1. Gross, S. P., Tuma, M. C., Deacon, S. W., Serpinskaya, A. S., Reilein, A. R. & Gelfand, V. I. (2002) *J. Cell Biol.* **156,** 855–865.
2. Rodionov, V., Yi, J., Oladipo, A., Kashina, A. & Gross, S. P. (2003) *Curr. Biol.* **13,** 1837–1847.
3. Steyer, J. A. & Almers, W. (1999) *Biophys. J.* **76,** 2262–2271.
4. Wong, I. Y., Gardel, M. L., Reichman, D. R., Weeks, E. R., Valentine, M. T., Bausch, A. R. & Weitz, D. A. (2004) *Phys. Rev. Lett.* **92**, 178101–178104.
5. Wu, X. & Libchaber, A. (2000) *Phys. Rev. Lett.* **84,** 3017–3020.
6. Weeks, E. R. & Swinney, H. L. (1998) *Phys. Rev. E* **57,** 4915–4920.
7. Newman, M. E. J. (2003) *SIAM Rev.* **45,** 167–256.
8. Mehta, A. D., Rock, R. S., Rief, M., Spudich, J. A., Mooseker, M. S. & Cheney, R. E. (1999) *Nature* **400**, 590–593.
9. Berg, H. (1993) *Random Walks in Biology* (Princeton Univ. Press, Princeton).
10. Yildiz, A., Forkey, J. N., McKinney, S. A., Ha, T., Goldman, Y. E. & Selvin, P. R. (2003) *Science* **300,** 2061–2065.
11. Ashkin, A., Schutze, K., Dziedzic, J. M., Euteneuer, U. & Schliwa, M. (1990) *Nature* **348,** 346–348.
12. Gross, S. P., Welte, M. A., Block, S. M. & Wieschaus, E. F. (2002) *J. Cell Biol.* **156,** 715–724.
13. Visscher, K., Schnitzer, M. J. & Block, S. M. (1999) *Nature* **400,** 184–189.
14. Vale, R. D., Malik, F. & Brown, D. (1992) *J. Cell Biol.* **119,** 1589–1596.
15. Tanaka, H., Homma, K., Iwane, A. H., Katayama, E., Ikebe, R., Saito, J., Yanagida, T. & Ikebe, M. (2002) *Nature* **415,** 192–195.
16. Evans, L. L., Lee, A. J., Bridgman, P. C. & Mooseker, M. S. (1998) *J. Cell Sci.* **111,** 2055–2066.
17. Nascimento, A. A., Amaral, R. G., Bizario, J. C., Larson, R. E. & Espreafico, E. M. (1997) *Mol. Biol. Cell* **8,** 1971–1988.
18. Wu, X., Bowers, B., Wei, Q., Kocher, B. & Hammer, J. A. III (1997) *J. Cell Sci.* **110**, 847–859.
19. Lewis, A. K. & Bridgman, P. C. (1992) *J. Cell Biol.* **119,** 1219–1243.
20. Lakadamyali, M., Rust, M. J., Babcock, H. P. & Zhuang, X. (2003) *Proc. Natl. Acad. Sci. USA* **100**, 9281–9285.
21. Svitkina, T. M. & Borisy, G. G. (1998) *Methods Enzymol.* **298,** 570–592.